

Scroll wave with negative filament tension in a model of the left ventricle of the human heart and its overdrive pacing

Sergei F. Pravdin ^{1,2,*}, Timofei I. Epanchintsev ^{1,2}, Hans Dierckx ³, and Alexander V. Panfilov ^{4,5,6}

¹*Krasovskii Institute of Mathematics and Mechanics, 620108 Ekaterinburg, Russia*


²*High-Performance Computing Department, Ural Federal University, 620002 Ekaterinburg, Russia*

³*KU Leuven Campus Kortrijk–Kulak, 8500 Kortrijk, Belgium*

⁴*Research Laboratory “Mathematical Modeling in Physiology and Medicine Based on Supercomputers”, Ural Federal University, 620002 Ekaterinburg, Russia*

⁵*Ghent University, 9000 Ghent, Belgium*

⁶*World-Class Research Center “Digital biodesign and personalized healthcare,” I.M. Sechenov First Moscow State Medical University, 119146 Moscow, Russia*

 (Received 19 April 2021; revised 4 August 2021; accepted 18 August 2021; published 10 September 2021)

Nonlinear waves of electrical excitation initiate cardiac contraction. Abnormal wave propagation in the heart, e.g., spiral waves, can lead to sudden cardiac arrest. This study analyzed the dynamics of spiral waves under the influence of an instability called negative filament tension, and examined how the spiral waves can be eliminated through high-frequency pacing. A generic anatomical model of the left ventricle of the human heart and the Aliev–Panfilov model for cardiac tissue were used. The study showed that the source of such arrhythmia is elongated filaments with lengths that can be 10–20 times greater than the characteristic thickness of the heart wall. In anisotropic tissue, the filament elongated before it was annihilated at the base of the heart. The spiral waves were eliminated through overdrive pacing with stimulation periods from 0.8 to 0.95 relative to the spiral wave period. The minimum time for the expulsion was about 10 s.

DOI: [10.1103/PhysRevE.104.034408](https://doi.org/10.1103/PhysRevE.104.034408)

I. INTRODUCTION

Nonlinear waves occur in various physical, chemical, and biological systems and can control their important properties [1]. For example, nonlinear electrical waves of excitation propagate through the human heart and initiate its contraction. Such waves can also form self-sustaining vortices which induce dangerous cardiac arrhythmias. The centers of rotation of a vortex in a three-dimensional (3D) medium form a line, called a filament. In some cases, the formation of vortices leads to complex chaotic spatiotemporal regimes in the heart, which disorganizes cardiac contraction and causes a sudden cardiac arrest. Mechanisms by which such chaotic regimes occur are still not completely understood, and one of the widely discussed hypotheses connects these regimes to the so-called negative filament tension.

The tension coefficient b_2 links the filament length l and curvature k , which for a circular filament of radius R and curvature $k = 1/R$ can be written as $dR/dt = -b_2/R$ [2]. A filament with a positive tension reduces its radius or—in the case of general shape—shortens. A filament with a negative tension tends to increase its length, and therefore tends to buckle and curl.

Before the tension concept was proposed, the extension of a circular filament with, actually, a negative tension was numerically demonstrated for the first time in Ref. [3], and buckling of filaments in some cases was hypothesized [4].

Such elongation is a result of the instability of the filament with respect to perturbations that induce its curvature. This hypothesis was actively discussed after a seminal paper by Winfree [5], who stated that ventricular fibrillation should be an essentially 3D phenomenon. An asymptotic theory for filament dynamics was developed by Biktashev *et al.* [2].

It is important to study conditions of disappearance of scroll waves. The disappearance can be spontaneous, due to filament drift and collision, for example, or induced by an external action. Scroll waves with a negative filament tension can be eliminated if a model parameter is periodically varied in time and the model stays in the area of the negative tension [6]. In spite of its importance, mechanisms of inducing drift of scroll waves with the negative tension have not yet been studied in an anatomical model of the heart. However, the study in a realistic geometry is very important, as the shape and properties of the domain such as thickness or the curvature of its boundary are essential for the development of instability. In addition, anatomically correct anisotropy of the tissue is another important factor in filament dynamics [7].

Since a main motivation for cardiac modeling is to find methods of stopping the arrhythmia, methods of controlling or eradicating spiral waves have also been investigated in previous studies. Currently, fibrillation is usually treated with a traditional electrical shock with a voltage of several kilovolts, which is effective but painful and can damage the patient’s heart. An alternative treatment is low-voltage, high-frequency overdrive pacing of the heart with a period less than that of the arrhythmia, which is also called antitachycardia pacing. This method is based on the phenomenon of induced drift of spiral

*Corresponding author: sfpravdin@imm.uran.ru

waves interacted with plane waves from a periodically excited source, which was first described in Ref. [8] for an active chemical medium. In our previous papers, we studied this process, which we will refer to as low-voltage cardioversion (LVC), in two-dimensional (2D) models of the myocardium. We considered a simple two-variable Aliev–Panfilov model [9] in the isotropic medium [10,11], an anisotropic medium with straight fibers and mechanoelectrical feedback [12], a Luo–Rudy I model [13,14], and a ten Tusscher–Panfilov model, TP06 [15]. However, the LVC has been studied in 3D anatomical models of the heart only for the positive filament tension [16].

This study investigates the feasibility of LVC in a 3D anatomical anisotropic representation of the myocardial wall in cases with negative-tension filaments. The left ventricle (LV) is an important region of the heart to simulate in three dimensions. To find out the fundamental effects of LVC in this heart chamber, the authors' previously developed generic model of the LV, which correctly reproduces its shape and anisotropy [17], was used. Scroll waves whose filaments elongated due to negative tension were initiated, and this process is reported as it significantly depends on the chosen anisotropy ratio of the tissue. Thereafter, low-voltage overdrive pacing was applied in this anatomical model, and pacing frequencies for which the LVC was successful are reported. Finally, it is discussed if the observed numerical phenomena (with and without pacing) are in line with existing theories on filament dynamics.

This paper is structured as follows. Section II describes the methods used for the simulation, scroll wave initiation, overdrive pacing, and analysis of the results. The numerical results are presented in Sec. III, for the cases with and without pacing. In Sec. IV, our observations are linked to the existing theories, and limitations and future extensions of the study approach are discussed.

II. METHODS

A. Left-ventricular geometry model

This study considered spiral waves in an axisymmetric LV because their dynamics are rich and incompletely understood even in the simplified case. The mathematical formulation of the LV has been developed before [17], in terms of curvilinear coordinates, wherein $\psi \in [0, \pi/2]$ indicates the relative position between the cardiac base (the widest open upper part of the LV model) and the apex (the bottom of the LV), $\gamma \in [\gamma_0, \gamma_1]$ indicates the position between the endocardium and the epicardium, and $\phi \in [0, 2\pi]$ is the circumferential coordinate.

The LV shape model has the following parameters. The wall thickness at the base, L ; the transverse radius of the LV cavity at the base, r_b ; the outer LV radius at the base, $R_b = r_b + L$; the cavity height z_b ; the apical wall thickness h ; the axial LV length $Z_b = z_b + h$; and the shape factor $\epsilon \in [0, 1]$. The coordinate transformation between the curvilinear and Cartesian coordinates is given by the following equations [17]:

$$x = \rho(\gamma, \psi) \cos \phi, \quad (1)$$

$$y = \rho(\gamma, \psi) \sin \phi, \quad (2)$$

$$z = (z_b + \gamma h)(1 - \sin \psi) + (1 - \gamma)h, \quad (3)$$

$$\rho(\gamma, \psi) = (r_b + \gamma L)(\epsilon \cos \psi + (1 - \epsilon)(1 - \sin \psi)). \quad (4)$$

Further, parameters γ_0 and γ_1 are used to define the fiber directions on the epicardium and the endocardium. Using these two parameters, we scaled the effective parameters (with index e) and obtained the formal parameters:

$$R_b = R_b^e + \frac{L^e \gamma_0}{\gamma_1 - \gamma_0}, \quad (5)$$

$$L = \frac{L^e}{\gamma_1 - \gamma_0}, \quad (6)$$

$$r_b = r_b^e - \frac{L^e(1 - \gamma_1)}{\gamma_1 - \gamma_0}, \quad (7)$$

$$Z_b = Z_b^e + \frac{h^e \gamma_0}{\gamma_1 - \gamma_0}, \quad (8)$$

$$h = \frac{h^e}{\gamma_1 - \gamma_0}, \quad (9)$$

$$z_b = Z_b - h, \quad (10)$$

$$\phi_{\max} = \frac{\phi_{\max}^e}{\gamma_1 - \gamma_0}. \quad (11)$$

Here, $\phi_{\max} > 0$ is the spiral surface rotation angle (it influences fiber directions and lengths). The parameter values that represented well the shape of an average human LV in norm were taken from [17] and are listed in Table I. Three LV shape models were examined by changing the apical LV wall thickness h^e to 6 mm so that the apex would be the thinnest place in the LV, to 12 mm so that the base would be as thick as the apex, and to 18 mm so that the LV base would be the thinnest place.

Anisotropic wave propagation was included by defining the local fiber directions. Since the fibers had to cover a 3D volume, they were a two-parametric family of curves. The first parameter, $\phi_0 \in [0, 2\pi]$, enabled copying of the fiber around the symmetry axis of the LV. The second parameter, $Y \in [0, K]$ with $K = R_b \phi_{\max} / \pi$, determined how closely the fiber approached the apex.

Each fiber was parametrized with $X \in [-\sqrt{K^2 - Y^2}, \sqrt{K^2 - Y^2}]$. Based on X and Y , $P = \sqrt{X^2 + Y^2}$ and $\Phi = \text{atan2}(Y, X)$ were computed. Based on P and Φ , the fiber coordinates in the LV model were computed:

$$\rho(P, \Phi) = \frac{P\pi}{\phi_{\max}} \left(1 - \frac{\Phi L}{\pi R_b} \right), \quad (12)$$

$$\phi(P, \Phi) = \phi_{\max} \frac{\Phi}{\pi} + \phi_0. \quad (13)$$

Finally, the other coordinates γ , z , and ψ were calculated as follows:

$$\gamma = (\phi - \phi_0) / \phi_{\max}, \quad (14)$$

$$s = \frac{\rho}{r_b + \gamma L}, \quad (15)$$

$$\mathcal{F} = \frac{\epsilon^2 + s(1 - \epsilon) - \epsilon \sqrt{2s(1 - \epsilon) + \epsilon^2 - s^2}}{(1 - \epsilon)^2 + \epsilon^2}, \quad (16)$$

TABLE I. Constant geometric model parameters.

Parameter	Variable	Value
Wall thickness at the base	L^e	12 mm
Transverse radius of the LV cavity at the base	r_b^e	21 mm
Axial LV length	Z_b^e	60 mm
Shape factor	ϵ	0.85
Outer LV radius at the base	R_b^e	33 mm
Spiral surface rotation angle	ϕ_{\max}^e	3π
Parameter to adjust the endocardial fiber directions	γ_0	0.1
Parameter to adjust the epicardial fiber directions	γ_1	0.9

$$z = (z_b + \gamma h)\mathcal{F} + (1 - \gamma)h, \tag{17}$$

$$\psi = \arcsin(1 - \mathcal{F}). \tag{18}$$

By differentiating each fiber with respect to the parameter X , the local unit fiber tangent $\hat{\mathbf{f}}$ was obtained. From this value, the 3×3 diffusion tensor \mathbf{D} was constructed as follows:

$$D_{ij}(\vec{r}) = D_2\delta_{ij} + (D_1 - D_2)f_i(\vec{r})f_j(\vec{r}), \tag{19}$$

where δ_{ij} is the Kronecker delta and f_i are the components of vector $\hat{\mathbf{f}}$ [18]. This expression is used below for the anisotropic diffusion of the excitation waves.

The myocardial fibers rotated in the wall, and their true fiber angle (the angle between the fiber tangent and the parallel $(-\sin \phi, \cos \phi, 0)$; see [17,19]) changed from -70° at the basal epicardium to $+70^\circ$ at the basal endocardium, so the total fiber rotation angle equaled 140° .

The parameter D_1 was kept constant so that the propagation velocity in the fiber direction would be the same in all the simulations. The diffusion coefficient transverse to the fiber, D_2 , was varied between simulations to test different anisotropy ratios as follows:

$$\eta = \frac{D_1}{D_2}. \tag{20}$$

The simulations were performed for $\eta \in \{1, 4, 9\}$. Since the propagation velocity in the spatial direction with the diffusivity D was scaled as \sqrt{D} , the anisotropy ratio in terms of the principal conduction velocities in the medium had the values of $c_1/c_2 \in \{1, 2, 3\}$.

Values of the main parameters are given in Tables I and II.

B. Model for excitation dynamics

We used the monodomain reaction-diffusion system of partial differential equations with Aliev–Panfilov kinetics [9]. These equations state how the normalized transmembrane po-

tential $u(\vec{r}, t)$ and an effective recovery variable $v(\vec{r}, t)$ change over time:

$$\frac{\partial u}{\partial t} = \vec{\nabla} \cdot (\mathbf{D}(\vec{r})\vec{\nabla}u) - ku(u - a)(u - 1) - uv + I_{\text{stim}}(\vec{r}, t), \tag{21}$$

$$\frac{\partial v}{\partial t} = -\left(\epsilon + \frac{\mu_1 v}{u + \mu_2}\right)(v + ku(u - b - 1)). \tag{22}$$

Here, \mathbf{D} is the electrical diffusion tensor from Eq. (19); $I_{\text{stim}}(\vec{r}, t)$ is the time-dependent stimulation current applied from an electrode and a, b, k, ϵ, μ_1 , and μ_2 are model parameters. The Laplacian operator was implemented in the curvilinear coordinates γ, ψ, ϕ (see [17] for details).

We used a variant of the Aliev–Panfilov model with parameters $k = 8, a = b = 0.1, \mu_1 = 0.2, \mu_2 = 0.3, \epsilon = 0.01$, and $D_1 = 0.05$. The same model was used in our two-dimensional (2D) simulations [10,20] so by comparing 2D and 3D results, we will be able to clearly see the effect of adding a spatial dimension.

We have previously measured the filament tension for this reaction kinetics parameter set (see [20]). In short, 2D isotropic simulations were performed, with an additional term $(1/R)\frac{\partial u}{\partial x}$, as if the filament were curved with radius $1/R$. If one takes $1/R$ constant in a simulation, then measuring the drift velocity in x and y directions allows the computation of the scalar and pseudoscalar filament tension coefficients [21]. The filament tension coefficient for this parameter set is $b_2 = -0.51$, appropriate for the present study of the negative tension behavior.

Although time is dimensionless in the Aliev–Panfilov model, it can be scaled to represent human ventricular activation [22]. In the model used in this study, the action potential duration at the 90% level was 25 time units. As the typical action potential duration in ionic models is around 300 ms [23], one model time unit (MTU) equals 12 ms. This value is used below to convert dimensionless time to (milli)seconds. The period of a spiral wave in the study model was $T_{\text{sw}} = 26$

TABLE II. Varied parameters.

Parameter	Variable	Values
Pacing period relative to spiral wave period	$T_{\text{stim}}/T_{\text{sw}}$	0.7, 0.75, ..., 1.0
Anisotropy ratio for the diffusion coefficients	η	1, 4, 9
Apical LV thickness	h^e	6, 12, 18 mm

MTU, which is equivalent to 312 ms. Spatial scaling was chosen based on the one-dimensional (1D) wave propagation speed $v_{1D} = 0.7$ mm/ms, so one model length unit (MLU) equaled 5.3 mm.

The minimal period of waves that can stably propagate (be assimilated) in a 1D fiber in this model is 17.5 MTU, or 0.67 relative to the spiral wave period. Only higher pacing periods should be examined in two and three dimensions as possible effective LVC periods.

C. Numerical simulation methods

Discretization. The LV shape was uniformly discretized in the curvilinear coordinates. For example, for the transmural coordinate γ , the interval was uniformly divided into $N_\gamma = 32$ sections, such that the corresponding index i_γ had values $0, 1, \dots, N_\gamma$. Similarly, $i_\psi \in \{0, 1, \dots, 152\}$ and $i_\phi \in \{0, 1, \dots, 419\}$.

Time stepping. Equations (21) and (22) were integrated using the forward Euler method, with $dt = 0.005$ MTU, which corresponds to 60 μ s.

Scroll wave initiation. A scroll wave was created by choosing appropriate initial conditions as follows:

$$u(i_\gamma, i_\psi, i_\phi) = \begin{cases} 1 & \text{if } i_\psi \leq 136 \text{ and } i_\phi \leq 34 \\ 0 & \text{otherwise,} \end{cases} \quad (23)$$

$$v(i_\gamma, i_\psi, i_\phi) = \begin{cases} k & \text{if } i_\psi \leq 136 \text{ and } 35 \leq i_\phi \leq 209 \\ 0 & \text{otherwise.} \end{cases} \quad (24)$$

These conditions initiated a fully transmural excited block in the medium that could not propagate to a higher ϕ because the medium was still refractory there.

Pacing protocol. The stimulation current which equaled I_{st} was applied at an area $\Omega_{stim} = \{(i_\gamma, i_\psi, i_\phi) | i_\psi > 136\}$ with a period T_{stim} by impulses with a duration $t_{stim} = 0.18$ MTU from a moment $t = \tau_0 = 100$ MTU (1200 ms). This can be written using Iverson brackets as

$$I_{stim}(i_\gamma, i_\psi, i_\phi, t) = I_{st}[(i_\gamma, i_\psi, i_\phi) \in \Omega_{stim}][t \geq \tau_0] \left[\left\{ \frac{t - \tau_0}{T_{stim}} \right\} \leq \frac{t_{stim}}{T_{stim}} \right], \quad (25)$$

where curly braces denote fractional part. Given a fixed impulse duration, we set the current as four times greater than the minimal current ($I_{min} = 0.75$) for exciting a fiber: $I_{st} = 4I_{min} = 3$.

Seven pacing periods were examined; they are listed in Table II. Combining these seven values with the three values for the anisotropy ratio η and the three values for the apical thickness, a total of 63 numerical simulations were performed.

Filament detection. Filaments were detected in the faces of the curvilinear grid. Each 1 MTU, or 12 ms, it was computed whether or not the isosurfaces $u = 0.5$ and $u_{prev} = 0.5$ intersected in that face, where u_{prev} is the potential 1 MTU earlier. No correction for anisotropy or curvature was made, and the medium was assumed to have been locally Euclidean during the filament detection.

Filament length calculation. The distances between all pairs of tips were computed. When we found a pair of tips

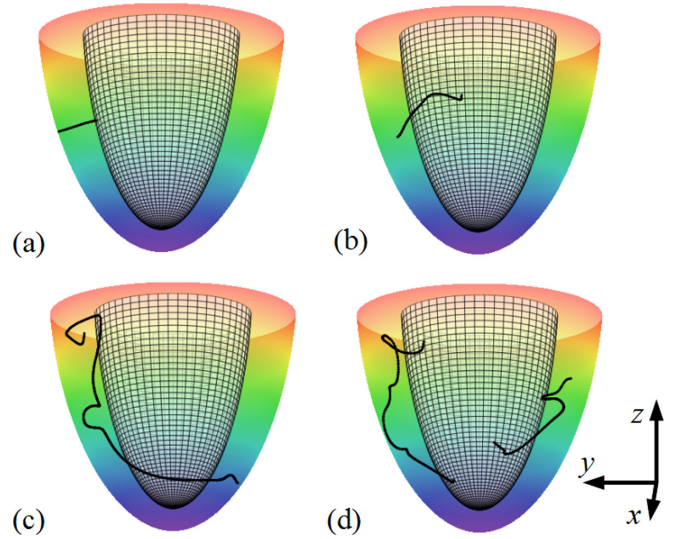


FIG. 1. Examples of scroll wave filaments without the low-voltage pacing. (a) Isotropy, $t = 21.5$ s; (b) anisotropy, $\eta = 4$, $t = 21.5$ s; (c) anisotropy, $\eta = 9$, $t = 12.2$ s; and (d) anisotropy, $\eta = 9$, $t = 22.4$ s. The epicardium is colored depending on the z coordinate. The mesh is the endocardium. The apical thickness is 6 mm.

that were closer than 0.001 MLU, we deleted one of them. A graph was made whose vertices were the tips. Two tips were connected by an edge if they were closer than 1 MLU. The graph connectivity components were found using the breadth-first search algorithm. Then the tips in each connectivity component were ordered into filaments using the NN-CRUST algorithm for curve (polyline) reconstruction [24]. Finally, the lengths of the polylines were calculated.

Criterion for successful LVC. Pacing was considered successful when no more tip was found at $t = 2000$ MTU (24 s) since the initial condition.

III. RESULTS

The observed dynamics with and without pacing are reported here. Then the observed results are explained using the theory of filament dynamics.

A. Scroll waves without pacing

In the absence of pacing, the three anisotropy ratios η yielded significantly different dynamics, as shown in Fig. 1.

In the isotropic case ($\eta = 1$) with all values of apical thickness, the filament was straight. When the apical thickness was 6 mm [see Fig. 1(a)], we observed a slow drift towards the LV base where the thickness of the wall was the largest. After that, the filament length remained constant in time (see Fig. 2). When the apex was 12 mm thick, the filament quickly drifted from the apical zone, where it was formed initially, to the middle LV zone ($\psi \approx 0.6$) and stayed there. In the LV model with an 18-mm-thick apex, the filament appeared in the apical zone first, then quickly moved to the same middle LV area and finally slowly drifted back towards the apex.

For moderate anisotropy ratio $\eta = 4$, regardless of the apical thickness, we observed a filament elongation and buckling [Fig. 1(b)].

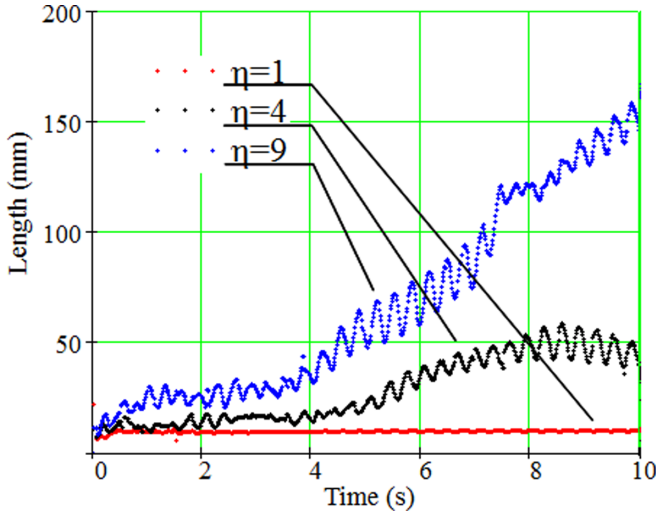


FIG. 2. Filament length (mm) versus time (s) for isotropic [red (light gray)] and anisotropic [black and blue (dark gray)] LV models without pacing. The apical thickness is 6 mm.

For the large anisotropy $\eta = 9$, the elongation notably increased, and the formation of a very long filament was observed. When the apical thickness was 6 mm, the filament was 150 mm long [see Figs. 1(c) and 1(d)]. In this case or when the apical thickness was 12 mm, the filament split when it collided with the epicardial or endocardial boundary, but no more than two filaments were observed at the same time. When the apical thickness was 18 mm, the scroll wave broke up and multiple (up to five during the first 15 s) long-buckled filaments appeared.

The filament length versus time over an interval of 10 s for the 6-mm-thick apex and all three anisotropy cases is shown in Fig. 2 (running medians filtering was applied to the length data to suppress outliers). An approximately constant length was seen for $\eta = 1$, an increase followed by a slow decrease for $\eta = 4$, and a growth of the filament for $\eta = 9$.

B. Effect of pacing

Next, we studied whether filaments with negative tension could be removed from the LV by external high-frequency pacing, for different stimulation periods and apical thicknesses as detailed in the methods section. Figure 3 shows a typical example of the scroll wave dynamics when the pacing was effective, with $T_{stim} = 22.1 = 0.85T_{sw}$, $h^e = 6$ mm. Similar to the 2D domains [10,20], the interaction consisted of two phases. In the first phase, the area excited by the electrode expanded and moved towards the filament (Fig. 3, left). When the external waves reached the filament, the latter moved away from the source and the induced drift began similarly to the 2D case. This drift made the filament shift from its initial position to the domain boundary (Fig. 3, right). Further details are shown in Fig. 4, where we depict the trajectory of the endocardial end of the filament, if this end existed, and several positions of the filament during its drift. The thicker lines correspond to the later time. We see that the high-frequency pacing in the isotropic LV shifted the filament to the base

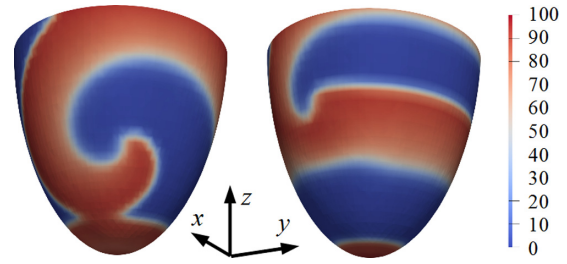


FIG. 3. High-frequency pacing of a scroll wave before (left, $t = 3$ s) and during (right, $t = 4.5$ s) the induced drift. Isotropic LV model with the apical thickness of 6 mm. Low-voltage pacing with the period $T_{stim} = 22.1$ MTU = 265 ms. The potential u is multiplied by 100 and color coded.

where it was annihilated. The filament maintained approximately the same shape and length during the drift.

The moderately anisotropic case $\eta = 4$, also with $T_{stim} = 22.1 = 0.85T_{sw}$, showed a similar drift to the base [Fig. 4(b)]. However, the filament dynamics were more complex; the filament initially elongated (filaments 3 and 4), then reached the LV base, shortened (not shown), and was annihilated.

The highly anisotropic case ($\eta = 9$) led to even more pronounced filament elongation [Fig. 4(c)]. The pacing limited the filament length to 90 mm, in comparison with 150 mm without the stimulation (Fig. 2), and caused a filament drift to the base and disappearance after 11 s.

Plots of length of the filaments versus time are shown in Fig. 5. In the two anisotropic cases, the filament length oscillated before $t = 3$ s [it was the first LVC phase when the scroll wave core had no contact with the wavetrain; see filament 1 in Fig. 4(b)]; then from $t = 3$ s to $t = 6$ s, the

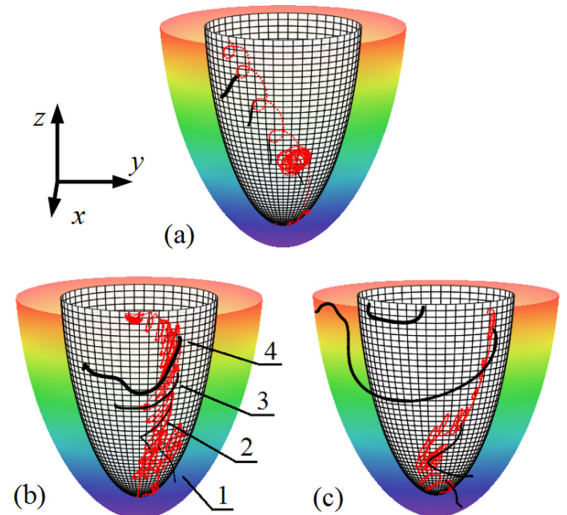


FIG. 4. Filament trajectories at the endocardium [red (gray) curves] and filament examples (black curves). (a) Isotropy, (b) moderate anisotropy ($\eta = 4$), and (c) high anisotropy ($\eta = 9$). Pacing period $T_{stim} = 22.1$ MTU, equal to $0.85T_{sw}$. The filaments are shown at different times, and the later filaments are closer to the base and drawn thicker. The apical thickness is 6 mm. In (b), labels 1–4 denote filaments at times 1.34, 4.4, 5.0, and 5.4 s that are referred to in the text.

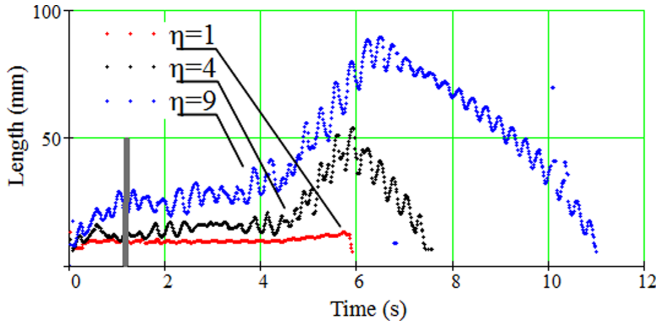


FIG. 5. Length of the filaments (mm) versus time (s). The high-frequency pacing with the period 22.1 MTUs is enabled. The gray line shows the moment when the pacing started. Isotropy [red (light gray)], moderate anisotropy $\eta = 4$ (black), and high anisotropy $\eta = 9$ [blue (dark gray)]. The apical thickness is 6 mm.

filament became approximately three times longer [filaments 2–4 in Fig. 4(b)]. Finally, the length dropped to zero when the filament disappeared near the cardiac base. For the isotropic case, the length of the filament was approximately constant during its drift.

The pacing was effective for periods from 20.8 to 24.7 MTU (0.8–0.95 relative to the spiral wave period) regardless of the anisotropy ratio or the apical thickness. The stimulation with shorter periods caused dynamical instabilities far from the electrode. Such a phenomenon has already been reported [15] for the TP06 model and a 2D isotropic domain. This implies that the wave from the electrode could not propagate into a certain area and caused the wavefront to break up and create new filaments. The pacing was ineffective and the spiral wave suppressed the waves from the electrode when $T_{\text{stim}} = T_{\text{sw}}$.

C. Theoretical explanation of observed results

Filament dynamics without pacing. The observed dynamics without pacing are consistent with the existing theory on buckling of scroll waves [25]. The cited study showed that for the negative tension instability to develop, a minimum wall thickness L_c is necessary.

Lowering the diffusion coefficient led to a larger effective length [26,27]. Since the fibers were approximately parallel to the epicardial and endocardial surfaces, the transmural diffusion coefficient was D_2 , such that the effective wall thickness was

$$L_{\text{eff}} = L_0 \sqrt{\eta}, \quad (26)$$

where L_0 is the Euclidean wall thickness, which can be approximated for almost straight filaments by the total filament length.

The numerical results indicate that for the case $\eta = 1$, $L_{\text{eff}} < L_c$ such that the filament remained locally straight. For the second case, $\eta = 4$ [Fig. 1(b)] corresponded to a buckled filament, i.e., $L_{\text{eff}} \gtrsim L_c$. When the effective wall thickness was further increased ($\eta = 9$), the negative tension instability occurred and multiple filaments were created by the collision of a portion of the filament with the medium boundary.

Filament dynamics under pacing. It was noted that the filament oriented itself approximately in planes with a constant

Z (see Fig. 4) during the pacing, in contrast to the unpaced case, in which the buckled filaments ($\eta = 4, 9$) extended significantly more in the apex-base direction (see Fig. 1).

Such behavior can be explained by a recent theoretical result [28] stating that a paced filament will orient itself parallel to the impeding wave fronts emitted by the pacing site. Comparing the filament shape in Fig. 1(c) with those in Fig. 4(c) shows that the paced filament was extended more in the circumferential direction, whereas the unpaced filament was extended more in the apex-base direction. Since the pacing site was located at the apex, the impeding waves pushed the filament to become parallel to them, which explains the overall orientation of the filament in the circumferential direction.

Still, this alignment process was slow and, meanwhile, other “forces” acted on the filament, such as boundary repulsion, negative tension, and gradients in the wall thickness. However, finding a quantitative theory that fully explains this phenomenon is outside the scope of this study.

IV. DISCUSSION

The dynamics of unperturbed scroll waves in the LV model with a negative filament tension were studied, and the elimination of the scrolls through external high-frequency pacing was proposed. We performed our study on an anatomical model of the LV of the human heart and varied the degree of anisotropy. A new finding here is that, in the strongly anisotropic model, the filament substantially elongated up to 10–20 times longer than the typical thickness of the heart wall. The observed situation in Fig. 1(c) differs a lot from other types of electrical turbulence in the heart, which occur due to alternans instability [22,23], where on average about 20 filaments were constantly present in the heart. This elongation resulted in the formation of filaments roughly parallel to the endocardial and epicardial surfaces. This phenomenon can explain the breakthrough patterns on the cardiac surfaces during the ventricular arrhythmias in experiment [29].

Several factors are known to affect filament drift, such as the filament curvature, the interaction of the filament with the domain boundaries, the local anisotropy, and the myocardial wall thickness. However, this negative tension did not lead to a significant breakup of the filament, as the system exhibited repulsion between the filament and the medium boundaries, which prevented the filament from colliding with the boundaries and forming new U-shaped filaments. Such attraction or repulsion was described using response functions and boundary potentials [30,31].

The mechanistic interpretation of the results (Sec. III C) revealed that the filament buckling phenomenon [25] together with the effective wall thickness can explain the observed dynamics prior to the pacing. Another source of drift, gradients of the wall thickness, will only be relevant to nearly straight filaments, as such filaments can increase or decrease their length (a tendency arising from filament tension) through drifting. The filaments with a large buckling amplitude ($\eta = 4, 9$) did not significantly change in length under lateral drifting. Therefore, the drift induced by the thickness gradients ceased to play a primary role.

This study was conducted to investigate the effect of pacing on negative filament tension. Pacing was found to be successful independently of the anisotropy ratio, and the underlying mechanism was related to the slow alignment of the filament with the wave fronts formed by the impeding waves. However, a full quantitative explanation could not be given.

If spiral waves in a specific heart model are prone to breakup, there are breakup-inducing factors such as the domain dimension (if the model has a purely 3D breakup), medium anisotropy, a large heart chamber, and a thick heart wall. Furthermore, besides a spontaneous breakup, there are several LVC-hindering factors such as the domain dimension (a certain pacing period may be effective in two dimensions but ineffective in three dimensions [28]), an insufficient electrode size or pacing current [20], anisotropy [16], and a small difference between the minimum 1D assimilable pacing period and the spiral wave period [15]. The 2D results for the isotropic and anisotropic square domains [10,11,32] had the same effective pacing periods, which shows that the domain dimension, anisotropy degree, wall thickness gradient, and heart shape did not affect the interval in the parameter ranges examined in our studies.

Additional tests were performed with piecewise reaction kinetics in the Aliev–Panfilov model in a 3D slab [28]. In the cases with negative filament tension, the intervals did not match for the 2D squares and the 3D slabs. On the other hand, the similarity of the intervals in the 2D squares and 3D LVs for the smooth Aliev–Panfilov model ensures that the period interval of a successful LVC in a slab will be the same.

In the anisotropic models, a phase was observed when the length of the filament initially increased before the filament was annihilated at the LV base. Even filaments with a positive tension may grow if they are pinned to inexcitable heterogeneities, as chemical experiments for the Belousov–Zhabotinsky reaction [33] and simulations for the Barkley

model with inert knots in the medium [34] have shown. Filaments with negative tension can grow and buckle but stay few in number in a domain thick enough for buckling but below a certain thickness [35].

Existence of negative filament tension should also be studied in experiment, as this is still a hypothesis now. Identification of filament in the heart is an extremely difficult problem. However, new experimental methods have been developed recently [36], which makes it possible to study filament dynamics in experiment.

One limitation of this study is that high-frequency pacing was investigated only for a symmetric LV geometry. However, the obtained examples are considered the most representative, as the chosen geometry with the thin apex is close to that of the normal human heart. In addition, similar studies on scroll waves in a physiologically heterogeneous medium (their unpaced dynamics were considered in Ref. [37]), using a detailed ionic cell-level model, as was done in Ref. [38], and with a vanishing filament tension, as in Ref. [39], should be performed.

Negative filament tension does not seem to limit LVC in the LV of the human heart even when the cardiac wall is thicker than normal.

ACKNOWLEDGMENTS

Our work involved simulations at the “Uran” cluster of IMM UB RAS (Ekaterinburg). Our research is supported by a Russian Science Foundation grant (Project 17-71-20024).

S.F.P. participated in the simulations, data analysis, and writing of Secs. I, II, III A, III B, and IV. T.I.E. participated in the simulations for Secs. III A and III B. H.D. participated in the data analysis, interpretation of the results, and writing of the paper, and developed the theoretical framework in Sec. III C. A.V.P. proposed and supervised numerical parts of the research and participated in writing the paper.

-
- [1] A. T. Winfree and S. H. Strogatz, Organizing centers for three-dimensional chemical waves, *Nature (London)* **311**, 611 (1984).
 - [2] V. N. Biktashev, A. V. Holden, and H. Zhang, Tension of organizing filaments of scroll waves, *Philos. Trans. R. Soc. A* **347**, 611 (1994).
 - [3] A. V. Panfilov and A. N. Rudenko, Two regimes of the scroll ring drift in the three-dimensional active media, *Phys. D* **28**, 215 (1987).
 - [4] P. K. Brazhnik, V. A. Davydov, V. S. Zykov, and A. S. Mikhailov, Vortex rings in excitable media, *Zh. Eksp. Teor. Fiz.* **93**, 1725 (1987).
 - [5] A. Winfree, Electrical turbulence in three-dimensional heart muscle, *Science* **266**, 1003 (1994).
 - [6] S. Alonso, F. Sagués, and A. S. Mikhailov, Taming Winfree turbulence of scroll waves in excitable media, *Science* **299**, 1722 (2003).
 - [7] H. Verschelde, H. Dierckx, and O. Bernus, Covariant Stringlike Dynamics of Scroll Wave Filaments in Anisotropic Cardiac Tissue, *Phys. Rev. Lett.* **99**, 168104 (2007).
 - [8] V. Krinsky and K. Agladze, Interaction of rotating waves in an active chemical medium, *Physica D* **8**, 50 (1983).
 - [9] R. Aliev and A. Panfilov, A simple two-variable model of cardiac excitation, *Chaos, Solitons Fractals* **7**, 293 (1996).
 - [10] S. F. Pravdin, T. V. Nezlobinsky, and A. V. Panfilov, Modelling of low-voltage cardioversion using 2D isotropic models of the cardiac tissue, in *Proceedings of the International Conference Days on Diffraction 2017* (IEEE, New York, 2017), pp. 276–281.
 - [11] E. Kuklin and S. Pravdin, In-silico analysis of the role of boundary conditions in the induced drift of 2D spiral waves, in *2020 Ural Symposium on Biomedical Engineering, Radioelectronics and Information Technology (USBEREIT)* (IEEE, New York, 2020), pp. 81–84.
 - [12] S. F. Pravdin and A. V. Panfilov, Optimization of a cardiac electromechanics simulation program for parallel implementation, in *2019 International Multi-Conference on Engineering, Computer and Information Sciences (SIBIRCON)* (IEEE, New York, 2019), pp. 768–774.

- [13] T. Epanchintsev, S. Pravdin, and A. Panfilov, Spiral wave drift induced by high-frequency forcing. Parallel simulation in the Luo–Rudy anisotropic model of cardiac tissue, in *Computational Science - ICCS 2018*, Lecture Notes in Computational Science and Engineering Vol. 10860 (Springer, Berlin, 2018), pp. 378–391.
- [14] T. Epanchintsev, S. Pravdin, and A. Panfilov, Simulation of spiral wave superseding in the Luo–Rudy anisotropic model of cardiac tissue with circular-shaped fibres, *J. Comput. Sci.* **32**, 1 (2019).
- [15] S. F. Pravdin, T. I. Epanchintsev, and A. V. Panfilov, Overdrive pacing of spiral waves in a model of human ventricular tissue, *Sci. Rep.* **10**, 20632 (2020).
- [16] S. F. Pravdin, T. I. Epanchintsev, T. V. Nezhlobinskii, and A. V. Panfilov, Induced drift of scroll waves in the Aliev–Panfilov model and in an axisymmetric heart left ventricle, *Russ. J. Numer. Anal. Math. Modell.* **35**, 273 (2020).
- [17] S. F. Pravdin, V. I. Berdyshev, A. V. Panfilov, L. B. Katsnelson, O. Solovyova, and V. S. Markhasin, Mathematical model of the anatomy and fibre orientation field of the left ventricle of the heart, *Biomed. Eng. Online* **12**, 54 (2013).
- [18] R. H. Keldermann, K. H. W. J. ten Tusscher, M. P. Nash, C. P. Bradley, R. Hren, P. Taggart, and A. V. Panfilov, A computational study of mother rotor VF in the human ventricles, *Am. J. Physiol. Heart Circ. Physiol.* **296**, H370 (2009).
- [19] D. D. J. R. Streeter, Gross morphology and fiber geometry of the heart, in *Handbook of Physiology* (American Physiological Society, Bethesda, MD, 1979), Vol. I, pp. 61–112.
- [20] S. F. Pravdin, T. V. Nezhlobinsky, and A. V. Panfilov, Inducing drift of spiral waves in 2D isotropic model of myocardium by means of an external stimulation, in *Proceedings of the 48th International Youth School-Conference “Modern Problems in Mathematics and its Applications,” CEUR-WS*, Vol. 1894 (IMM UB RAS, Yekaterinburg, Russia, 2017), pp. 268–284.
- [21] A. V. Panfilov and A. V. Holden, Computer simulation of re-entry sources in myocardium in two and three dimensions, *J. Theor. Biol.* **161**, 271 (1993).
- [22] A. V. Panfilov, Three-dimensional organization of electrical turbulence in the heart, *Phys. Rev. E* **59**, R6251 (1999).
- [23] R. H. Keldermann, K. H. W. J. ten Tusscher, M. P. Nash, R. Hren, P. Taggart, and A. V. Panfilov, Effect of heterogeneous APD restitution on VF organization in a model of the human ventricles, *Am. J. Physiol. Heart Circ. Physiol.* **294**, H764 (2008).
- [24] T. K. Dey and P. Kumar, A simple provable algorithm for curve reconstruction, in *Proceedings of the Tenth Annual ACM-SIAM Symposium on Discrete Algorithms*, SODA '99 (Society for Industrial and Applied Mathematics, Philadelphia, 1999), pp. 893–894.
- [25] H. Dierckx, H. Verschelde, O. Selsil, and V. N. Biktashev, Buckling of Scroll Waves, *Phys. Rev. Lett.* **109**, 174102 (2012).
- [26] R. J. Young and A. V. Panfilov, Anisotropy of wave propagation in the heart can be modeled by a Riemannian electrophysiological metric, *Proc. Natl. Acad. Sci. USA* **107**, 15063 (2010).
- [27] M. Wellner, O. Berenfeld, J. Jalife, and A. M. Pertsov, Minimal principle for rotor filaments, *Proc. Natl. Acad. Sci. USA* **99**, 8015 (2002).
- [28] S. F. Pravdin, T. V. Nezhlobinsky, A. V. Panfilov, and H. Dierckx, High-frequency pacing of scroll waves in a three-dimensional slab model of cardiac tissue, *Phys. Rev. E* **103**, 042420 (2021).
- [29] A. V. Zaitsev, O. Berenfeld, S. F. Mironov, J. Jalife, and A. M. Pertsov, Distribution of excitation frequencies on the epicardial and endocardial surfaces of fibrillating ventricular wall of the sheep heart, *Circ. Res.* **86**, 408 (2000).
- [30] V. N. Biktashev and A. V. Holden, Resonant drift of autowave vortices in two dimensions and the effects of boundaries and inhomogeneities, *Chaos, Solitons Fractals* **5**, 575 (1995).
- [31] C. D. Marcotte and R. O. Grigoriev, Unstable spiral waves and local Euclidean symmetry in a model of cardiac tissue, *Chaos* **25**, 063116 (2015).
- [32] T. Epanchintsev, S. Pravdin, A. Sozykin, and A. Panfilov, Simulation of overdrive pacing in 2D phenomenological models of anisotropic myocardium, in *Proceedings of the Sixth International Young Scientists Conference in HPC and Simulation YSC 2017*, Procedia Computer Science, Vol. 119 (Elsevier, Kotka, Finland, 2017), pp. 245–254.
- [33] Z. A. Jiménez and O. Steinbock, Scroll wave filaments self-wrap around unexcitable heterogeneities, *Phys. Rev. E* **86**, 036205 (2012).
- [34] D. Weingard, O. Steinbock, and R. Bertram, Expansion of scroll wave filaments induced by chiral mismatch, *Chaos* **28**, 045106 (2018).
- [35] S. Alonso, M. Bär, and A. V. Panfilov, Negative tension of scroll wave filaments and turbulence in three-dimensional excitable media and application in cardiac dynamics, *Bull. Math. Biol.* **75**, 1351 (2012).
- [36] J. Christoph, M. Chebbok, C. Richter, J. Schröder-Schetelig, P. Bittihn, S. Stein, I. Uzelac, F. H. Fenton, G. Hasenfuß, R. F. Gilmour, and S. Luther, Electromechanical vortex filaments during cardiac fibrillation, *Nature (London)* **555**, 667 (2018).
- [37] P. V. Kononov, S. F. Pravdin, O. E. Solovyova, and A. V. Panfilov, Scroll wave dynamics in a model of the heterogeneous heart, *JETP Lett.* **104**, 130 (2016).
- [38] S. F. Pravdin, H. Dierckx, and A. V. Panfilov, Effect of the form and anisotropy of the left ventricle on the drift of spiral waves, *Biophysics* **62**, 391 (2017).
- [39] S. F. Pravdin, H. Dierckx, and A. Panfilov, Drift of scroll waves of electrical excitation in an isotropic model of the cardiac left ventricle, *Russ. J. Numer. Anal. Math. Modell.* **31**, 293 (2016).